IPHV8I2015X
International Journal Of Advanced Research and Innovation -Vol.8, Issue .II
ISSN Online: 2319 – 9253
Print: 2319 – 9245

COMPRESSIVE FLUORESCENCE MICROSCOPY FOR BIOLOGICAL AND HYPER SPECTRAL IMAGING

[#1]R.KAVYASREE, M.Tech student,
[#2]CH.KARUNA, Assistant Professor,
Dept of ECE,
SAHAJA INSTITUTE OF TECHNOLOGY & SCIENCES FOR WOMEN, KARIMNAGAR, TS, INDIA.

ABSTRACT: The mathematical theory of compressed sensing (CS) asserts that one can acquire signals from measurements whose rate is much lower than the total bandwidth. Whereas the CS theory is now well developed, challenges concerning hardware implementations of CS-based acquisition devices—especially in optics—have only started being addressed. This paper presents an implementation of compressive sensing in fluorescence microscopy and its applications to biomedical imaging. Our CS microscope combines a dynamic structured wide-field illumination and a fast and sensitive single-point fluorescence detection to enable reconstructions of images of fluorescent beads, cells and tissues with under sampling ratios (between the number of pixels and number of measurements) up to 32. We further demonstrate a hyper spectral mode and record images with 128 spectral channels and under sampling ratios up to 64, illustrating the potential benefits of CS acquisition for higher dimensional signals which typically exhibits extreme redundancy. Altogether, our results emphasize the interest of CS schemes for acquisition at a significantly reduced rate and point out to some remaining challenges for CS fluorescence microscopy.

I.INTRODUCTION

Fluorescence microscopy is a fundamental tool in basic and applied biomedical research. Because of its optical sensitivity and molecular specificity, it is employed in an increasing number of applications which, in turn, are continuously driving the development of advanced microscopy systems that provide imaging data with ever higher spatio-temporal resolution and multiplexing capabilities. In fluorescence microscopy, one can schematically distinguish two kinds of imaging approaches, differing by their excitation and detection modalities [1]. In wide-field (WF) microscopy, a large sample area is illuminated and the emitted light is recorded on a multidetector array, such as a CCD camera. In contrast, in raster scan (RS) microscopy, a point excitation is scanned through the sample and a point detector is used to detect the fluorescence signal at each position. While very distinct in their implementation and applications, these imaging modalities have in common that the acquisition is independent of the information content of the image. Rather, the number of measurements, either serial in RS or parallel in WF, is imposed by the Nyquist-Shannon theorem. This theorem states that the sampling frequency (namely the inverse of the image pixel size) must be twice the bandwidth of the signal, which is determined by the diffraction limit of the microscope lens equal to $\lambda/2NA$ (λ is the optical wavelength and NA the objective numerical aperture). Yet, most images, including those of biological interest, can be described by a number of parameters much lower than the total number of pixels. In everyday's world, a striking consequence of this compressibility is the ability of consumer cameras with several megapixel detectors to routinely reduce the number of bits in a raw data file by an order of magnitude or two without substantial information loss. To quote from David Brady: "if it is possible to compress measured data, one might argue that too many measurements were taken" [2]. The recent mathematical theory of compressed or compressive sensing (CS – see [3, 4]) has addressed this challenge and shown how the sensing modality could be modified to reduce the sampling rate of objects which are sparse in the sense that their information content is lower than the total bandwidth or the number of pixels suggest. The fact that one can sample such signals non-adaptively and without much information loss—if any at all—at a rate close to the image information content (instead of the total bandwidth) has important consequences, especially in applications where sensing modalities are slow or costly. To be sure, the applications of CS theory to data acquisition are rapidly growing in fields as diverse as medical resonance imaging [5, 6], analog-to-digital conversion [7] or astronomy [8]. In optics, the interest in CS has been originally spurred by the demonstration of the so-called "single-pixel camera" [9]. Since then, reports have explored the potential of CS for visible and infrared imaging [10, 11], holography [12] or ghost imaging [13]. In microscopy, the feasibility of CS measurements has recently been demonstrated [14]. Altogether, these results open exciting prospects, notably for the important case of biomedical imaging. Having said this, there are very few results about the performance of CS hardware devices on relevant biological samples. As such samples often have low fluorescence, it is especially important to understand how the associated noise will affect the acquisition and reconstruction schemes. In this paper, we describe

IPHV8I2015X
International Journal Of Advanced Research and Innovation -Vol.8, Issue .II
ISSN Online: 2319 – 9253
Print: 2319 – 9245

Compressive Fluorescence Microscopy (CFM), a novel modality for fluorescence biological and hyper spectral imaging based on the concepts of CS theory. In CFM, the sample is excited with a patterned illumination and its fluorescence is collected on a point detector. Images are computationally reconstructed from measurements corresponding to a set of appropriately chosen patterns. Therefore, CFM benefits from many advantages associated with RS techniques, namely, high dynamic range, facilitated multiplexing, and wide spectral range (from the UV to the IR). In truth, the benefits of CS are particularly appealing in biology where fast, high-resolution and multicolor imaging is highly sought after. The paper is organized as follows. We begin by recalling the principles of CS theory for optical imaging. We then turn to the description of the practical implementation of CFM and of the sensing protocol. Our techniques are subsequently applied to image several relevant samples, including fluorescent beads, cultured cells and tissues. By extending our implementation, we further demonstrate the possibility of hyper spectral acquisition with up to 128 different spectral channels. A final contribution is a careful study of various noise trade-offs for CFM. We conclude the paper with a discussion of prospective CFM developments.

II.COMPRESSED SENSING FRAMEWORK

We wish to image a two-dimensional sample x = {x[i]}, a distribution of fluorescent probes, in which x[i] is the value of x at the pixel/location i (thus one can view pixel intensities x[i] as the coef- ficients of the image x in a basis of localized functions, namely, the Dirac basis). We represent this object in a basis W of our choosing and write

$$\mathbf{x} = \sum_{p} c[p]\mathbf{w_p} = \mathbf{Wc},$$

Where the wp's are (orthogonal) basis functions and the c[p]'s are the coefficients of x in the expansion. We say that the signal is K-sparse if at most K of these coefficients are nonzero. An empirical fact is that most images of interest are well approximated by K-sparse expansions with K much less than the number of pixels N, and this is the reason why data compression is effective; one can store and transmit quantization of the large coefficients, ignore the small ones, and suffer little distortion. In our imaging setup, we measure correlations between the image of interest x and sensing waveforms φk taken from another basis Φ; that is, we measure

$$y_k = \langle \mathbf{x}, \phi_\mathbf{k} \rangle = \sum_{i} x[i]\phi_k[i]. \quad (1)$$

Here, φk is an illumination or intensity pattern so that yk is obtained by collecting all the fluorescence corresponding to those pixels that have been illuminated on a single-point detector. Wide-field and point-like excitation are two extreme cases, corresponding respectively to a uniform sensing waveform (φk[i] = 1 for all i) and to a spike or Dirac waveform.

In its simplest form, CS theory asserts that if the signal x is sparse in the representation W, then only few measurements of the form [1] are sufficient for perfect recovery provided the sensing and representation waveforms, respectively φk and wp, are incoherent [4, 15]. Two systems are said to be incoherent if any element in one of the two cannot be expressed as a sparse linear combination of elements taken from the other. Formally, the coherence between two ortho bases W and Φ of R N is measured by the parameter μ(W, Φ) ranging between 1 and N:

$$\mu(\mathbf{W}, \mathbf{\Phi}) = N \max_{p,k} |\langle \mathbf{w_p}, \phi_\mathbf{k} \rangle|^2. \quad (2)$$

The Fourier and Dirac bases are in this sense maximally incoherent (we need many spikes to synthesize a sinusoid and vice versa) and μ = 1. On the opposite, two identical bases are maximally coherent and, in this case, μ = N. Hence, incoherence expresses the idea of the level of dissimilarity between any two representations of a signal. With this in mind, one perceives how each incoherent measurement—a projection on an element of the basis Φ—conveys a little bit of information about all the entries of the coefficient vector c. An important result in CS theory states that K-sparse signals can be recovered exactly from comparably few measurements in an incoherent system. Further, recovery is achieved by solving a tractable optimization program—a linear program. One solves

$$\min_{\mathbf{c}\in\mathbb{R}^N} \|\mathbf{c}\|_{\ell_1} \text{ subject to } y_k = \langle \phi_\mathbf{k}, \mathbf{Wc} \rangle, \text{ for all } k = 1 \ldots M. \quad (3)$$

When M measurements are chosen uniformly at random from the basis Φ, the recovery is exact with very high probability; that is, the solution sequence cˆ obeys xˆ = P p cˆ[p]wp = x, provided that

$$M \geq C\, \mu(\mathbf{\Phi}, \mathbf{W})\, K \log N, \quad (4)$$

Where C is a constant on the order of unity. This result emphasizes both the role of the coherence and the potential gain for large images due to the logarithmic dependence in the pixel size. For incoherent pairs, we only need on the order of K log N random samples. We have discussed sparse signals above for ease of exposition. However, the theory extends to approximately sparse signals and to noisy data. For instance, if the signal is well approximated by a Ksparse signal (some would say that it is compressible), then the reconstruction error is shown to be small. Further, the recovery is not sensitive to noise in the sense that the error degrades gracefully as the signal-to-noise ratio decreases. We refer to [16] and references therein for quantitative statements.

III.COMPRESSIVE FLUORESCENCE MICROSCOPY:

Implementation Experimental setup.

IPHV8I2015X
International Journal Of Advanced Research and Innovation -Vol.8, Issue .II
ISSN Online: 2319 – 9253
Print: 2319 – 9245

Our setup is based on a standard epifluorescence inverted microscope (Nikon Ti-E) as shown in Figure A. To generate spatially modulated excitation patterns, we incorporated a Digital Micro mirror Device (DMD) in a conjugate image plane of the excitation path. The DMD is a 1024-by-768 array of micro mirrors (Texas-Instrument Discovery 4100, Vialux, Germany) of size 13.68x13.68 µm each, and which can be shifted between two positions oriented at +12o or -12o with respect to the DMD surface. They are all independently configurable at frequency up to 20 kHz. The DMD is carefully positioned so that the optical axis (defined by the microscope lens and the dichroic mirror DM (Figure A)) is orthogonal to the plane of the DMD.

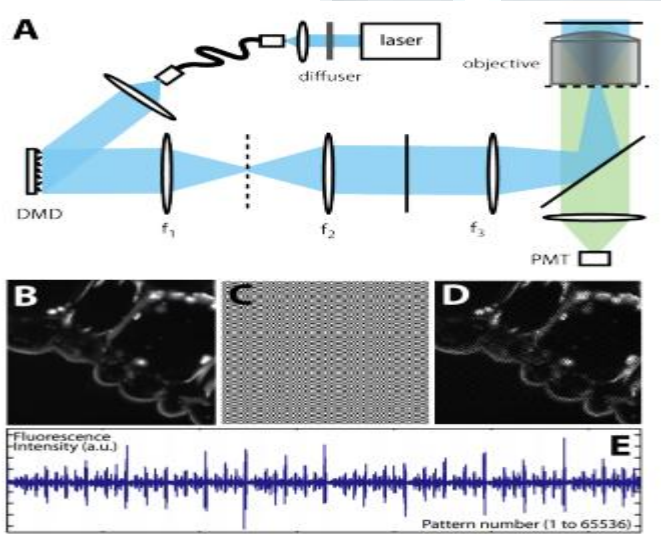

Fig. 1. (A) Experimental set-up. The dotted and plain segments correspond to planes respectively conjugated to the pupil and sample planes. (B) Slice of lily anther (endogenous fluorescence with epifluorescence microscopy image recorded on a CCD camera). (C) Projection of a Hadamard pattern on a uniform fluorescent sample. (D) Projection of the same Hadamard pattern on the biological sample. (E) Fluorescence intensity during an acquisition sequence.

As light source, we used a laser bench (Roper Scientific, France) equipped with two superimposed continuous-wave laser (λ=488 nm, Coherent, USA and λ=561 nm, Cobolt, Sweden). The laser beam first passed through a rotating diffuser or a phase scrambler (Dyoptika, Ireland) in order to reduce the spatial coherence and was then coupled to a 200µm multimode fiber. At the fiber output, the laser beam was expanded into a 2 cm diameter collimated beam. This beam was oriented towards the DMD at an angle of incidence corresponding to twice the tilting angle of the DMD mirrors (approx. 24o); a micromirror oriented at +12o would reflect the light into the microscope and appear as a bright pixel in the sample plane and, inversely, micro mirrors oriented at -12o appear as dark pixels. Depending on the samples, we used an air (Nikon, 20X, Plan Apo VC NA 0.75) or an oil-immersion objective (Nikon, 60X Plan Apo Tirf, NA 1.45). When the 20x air lens was used, the imaging lenses (lenses f1, f2, f3 in Figure A) were chosen to introduce a 1.5X reduction. The overall magnification of the image of the DMD on the sample was 1/30 and the size of a single micromirror equal to 456 nm. When the 60x lens was used, a different set of imaging lenses was chosen which only served as a 1x relay; here, the image size of a single micromirror in the sample plane was equal to 228 nm. Upon illumination with an intensity pattern (excitation intensity ~ 20 to 60 W/cm2), the sample fluorescence was detected on a photomultiplier tube PMT (Hamamatsu) and sampled at 96kHz using an analog-digital converter board (PCI-4462, National Instruments, USA) (Figure B-D). In CS measurements, the information on the sample is thus contained in the variations of the intensity signal as a function of the illumination pattern (Figure E). The WF image of the sample could also be directly formed on a camera (ImagEM, Hamamatsu, Japan) placed on the output port of the microscope. For hyperspectral imaging, the PMT was replaced by a fast and sensitive spectral detector described later in the paper. Note that the role of the DMD in our set-up differs from that in the "single-pixel camera" [9] or in some other microscopy setups [14]. In the latter, the modulator is placed between the sample and the detector, meaning that it is used to select some of the light within the total signal, rather than to control the excitation pattern. Our choice is motivated by the low level of fluorescence encountered in biological samples such as living cells labelled with fluorescent proteins. Indeed, the overall efficiency of a DMD is 68% and falls down to 34% when only one half of the mirrors are tilted. In our case, the photon collection efficiency is only limited by the numerical aperture of the microscope lens and the quantum yield of the detector as in conventional epifluorescence microscopy.

Choice of the illumination patterns.

For the practical implementation of a CS-based image acquisition system, it is essential to determine which incoherent basis should be used when no prior information on the signal is available. There are measurement ensembles, such as the partial Fourier or Hadamard systems, known to be highly incoherent with the bases in which most natural images are sparse. When excitation patterns are generated by micromirrors, φk[i] is a binary waveform taking on the two values 0 or 1. An appealing choice for Φ is then the Hadamard system known to be incoherent with the Dirac basis and fine scale wavelets. Since each entry of a Hadamard pattern hk is either −1 or +1, one defines φk as a shifted and rescaled version of hk via φk = (hk + 1)/2, which can be simply encoded on the DMD. We used patterns of size 256 × 256 and 128 × 128 obtained by binning 2 × 2 and 4 × 4 groups of micromirrors. The actual pattern h˜k formed in the sample plane is in fact the convolution of the ideal

pattern hk with the point spread function of the microscope Pexc in the excitation path. Figures C and D represent WF images of a Hadamard pattern projected on a uniform and on a biological sample. A specificity of optical imaging is that the sensing elements φk represent light intensities and are thus nonnegative which, as discussed later, has important practical implications. Hadamard waveforms have a sort of spatial frequency (like sinusoids) which grossly depends on the typical block size of the patterns. As the power spectrum of most biological images is generally concentrated at low frequencies, the flexibility in frequency selection is important. We introduce two distinct pattern selection strategies based on the expected spatial content of the sample:

- When the sample we wish to acquire is sparse in the pixel domain as in the case of single molecule or bead imaging, no typical frequency range needs to be favored and Hadamard patterns are selected uniformly at random.
- More complex samples have a power spectrum typically decaying like a power law. This a priori information suggests that we should balance low- and high-frequency measurements in order to accurately acquire the low-frequency part of the image, which accounts for a significant part of the total variance. The half-half strategy then projects the m/2 patterns with the lowest spatial frequencies to acquire a low-resolution image of the sample; the high-resolution content of the image is randomly sampled by choosing m/2 measurements among the N − m/2 remaining high-frequency Hadamard patterns. Such an adaptive strategy guarantees an accurate determination of the low-frequency content while allowing for the estimation of details at a finer scale.

Computational reconstruction.

In CS, it is essential to enforce the sparsity of the reconstructed signal in some representation W that is chosen a priori. The choice of W highly depends on the spatial structures of the signal to be reconstructed. One would typically use a Fourier representation for oscillatory features, wavelets for pointwise singularities, curvelets for contour-like or filamentary structures [17] and so on. One could also use a concatenation of all these representations. (If one intends on using the Fourier basis as a sparsity basis, one would need to scramble the columns of the Hadamard basis since it would otherwise be coherent with sinusoids.) After recording the fluorescence intensity during a sequence of up to 65536 consecutive patterns (Figure C), one can imagine recovering the signal x from these data by solving the optimization problem [3]. Because our measurements are noisy, it is actually better to relax the constraints into

$$\min_{x\in\mathbb{R}^N} \|\mathbf{W}^T\mathbf{x}\|_{\ell_1} \quad \text{subject to} \quad \|\mathbf{y}-\mathbf{\Phi x}\|_{\ell_2} \le \epsilon; \tag{5}$$

we ask that the fit holds up to the noise level. In the following, W will be either an ortho normal basis (e.g. Dirac basis) or an over complete signal representation (e.g. undecimated wavelet frame or curve let frame). This will be clearly specified for each individual reconstruction result. For computational reasons, we find it convenient to solve a relaxed version of this problem, namely,

$$\min_{x\in\mathbb{R}^N} \|\mathbf{W}^T\mathbf{x}\|_{\ell_1} + \frac{\alpha}{2}\|\mathbf{y}-\mathbf{\Phi x}\|^2_{\ell_2}. \tag{6}$$

As is well known, there is a value α() such that the two programs coincide. For our experiments, we used the NESTA solver [29] and the regularization parameter α is chosen empirically depending on the noise level. When the signal is nearly sparse and the noise level low, it is known that this program finds a reconstruction with a low mean squared error (MSE).

IV.SPARSE FLUORESCENCE IMAGES: BEADS, CELLS AND TISSUES

Fluorescent beads

We first tested our CS microscope (with the 20x objective) on a sample of fluorescent beads (diameter 2 µm, peak emission at 520 nm, Fluorospheres Invitrogen) deposited on a glass coverslip. At a low density of beads, the WF image is the superposition of a few fluorescence spots on a dark background, a signal similar to that of single molecule imaging data in biology [18]. As for the sparsity basis W, we obtained nearly equivalent results using the Dirac basis or a wavelet transform. Here we show images reconstructed with the wavelet transform and using a number of random 256 × 256 Hadamard patterns decreasing from 16384 down to 512.

(To be complete, we used a weighted `1 norm in eq. [6] where the weight of each coefficient is inversely proportional to scale.) In the following, the undersampling ratio is the ratio between the number N of pixels and the number M of measurements. As shown in Figure 2, most of the bead positions are recovered with undersampling ratios up to 64, corresponding to M ∼ 1.5% of N. At higher undersampling ratios, beads with low intensities are lost. To quantify the distorsion of the reconstructed image as a function of the undersampling ratio, we calculated the Peak Signal-toNoise Ratio, PNSR = 10 log(d 2 /MSE) where MSE = N −1 kxˆ − xrefk 2 2, the squared distance between the reconstructed image from all the 256×256 possible measurements and that which only uses a fraction. Above, d is the dynamical range of the reconstruction obtained from a full sample. As shown in Figure 2A, the PSNR decreases with the undersampling ratio (blue curve) and seems to reach a plateau at ratios above 64 where most of the beads

are lost. Since beads with low intensities are lost before brighter beads, we made a second set of measurements with an excitation light intensity divided by 100 to assess the effect of illumination on compression efficiency. The red curve in Figure 2A represents the PNSR of the reconstructed images as a function of the undersampling ratio. As expected, the PNSR is lower than that for the nominal illumination and reaches a plateau at an undersampling ratio of about 10, where almost all the beads are lost. This clearly shows that the distortion of the reconstructed image is strongly affected by the amount of detected fluorescent photons. Indeed at such low intensities, photon noise (also termed, shot noise) may be significant. To further explore the impact of photon noise on the compression efficiency, we performed numerical simulations on an artificial image of fluorescent beads made of 50 Gaussian spots (FWHM 3 pixels) randomly positioned in the field of view of size 256 × 256 pixels. The simulated nominal illumination intensity I0 was set so that the resulting flux (i.e. the sum of the signals over all the pixels) was equal to f0 = 6.4e3. Each measurement yk was then computed as one realization of a Poisson process with mean hφk, xi. Reconstructions are processed with intensities I0, I0/10 and I0/100 for a range of undersampling ratios between 2 and 64. As shown by the PSNR curves (Figure 2B), these simulations qualitatively reproduce the loss of compression efficiency for low-light levels but fail to quantitatively estimate the PSNR of the reconstructed images. This suggests that photon noise is not the only source of image degradation in our imaging system. A possible additional cause is the discrepancies between the theoretical patterns and the effective illumination profiles in the sample plane.

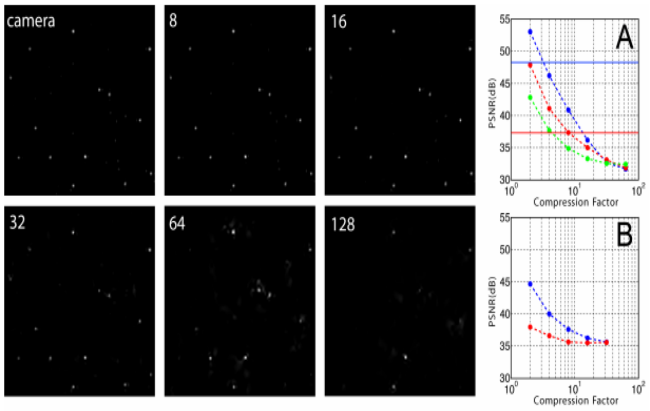

Fig. 2. Top left to bottom right: camera snapshot and reconstructed 256-by-256 bead images for values of the under sampling ratio equal to 8, 16, 32, 64 and 128. (A) Plot of the PSNR (see text) for a nominal illumination level (blue curve) and for the same level reduced by a factor 10 (red curve) and a factor of 100 (green curve) (simulated data). The solid lines correspond to the PSNR in raster scan for the same surfacic illumination. (B) Same as (A) for the experimental data.

V.CONCLUSION

This paper presented the principles and implementation of compressive sensing in fluorescence microscopy together with its applications in biomedical imaging. Our approach, which is based on a patterned excitation of the sample combined with a point-detection of the emitted fluorescence, readily allows for substantial undersampling gains when compared to traditional raster-scanning approaches. It could also be useful in situations, such as a diffusing media, where direct imaging on a multi-pixel detector is not possible. Furthermore, we have set forth a distinctive prospect for hyperspectral acquisition, which has great potential for multicolor single molecule imaging. More generally, the acquisition of 3D, 4D (three spatial dimensions and one spectral or temporal dimension) or even higher dimensional signals puts unrealistic constraints on system resources. It is indeed hard to imagine that one would want to sample such huge data cubes at rates anywhere close to the Shannon rate. The key is that multidimensional signals become increasingly redundant in the sense that their information content grows at a much lower rate than the number of voxels. For example, movies are comparably far more compressible than still pictures. Likewise, hyperspectral movies are far more redundant than monochromatic movies, and so on. Expressed differently, the ratio between the number of degrees of freedom and the number of voxels decreases very rapidly as the dimension increases. The extreme sparsity of higher dimensional signals cannot be ignored and we expect the advantages of CFM to become paramount in such applications.

REFERENCES:

1. Mertz J (2010) Introduction to optical microscopy (Roberts and Company Publishers).
2. Brady DJ (2010) Optical Imaging and Spectroscopy (Wiley).
3. Donoho DL (2006) Compressed sensing. IEEE Trans. Inform. Theory 52:1289–1306.
4. Candes E, Romberg J, Tao T (2006) Robust uncertainty principles: exact signal reconstruction from highly incomplete frequency information. IEEE Trans. Inform. Theory 52:489–509.
5. Lustig M, Donoho D, Pauly P (2007) Sparse MRI: The application of compressed sensing for rapid MR imaging. Magnetic Resonance in Medicine 58:1182–1195.
6. Trzasko J, Manduca A, Borisch B (2009) Highly undersampled magnetic resonance image reconstruction via homotopic `0 minimization. IEEE Trans. Medical Imaging 28:106–121.
7. Mishali M, Eldar YC, Dounaevsky O, Shoshan E (2011) Xampling: Analog to digital at sub-Nyquist rates. IET Cir. Dev. and Systems 5:8–20.

8. Bobin J, Starck JL, Ottensamer R (2008) Compressed Sensing in Astronomy. IEEE Journal of Selected Topics in Signal Processing 2:718–726.
9. Duarte MF, Davenport MA, Takhar D, Laska JN, Sun T, Kelly KF, araniuk RG (2008) Single-Pixel Imaging via Compressive Sampling. IEEE Signal Process. Mag. 25:83–91.
10. Pitsianis NP, Brady DJ, Portnoy A, Sun X, Suleski T, Fiddy MA, Feldman MR, Tekolste RD (2006) Compressive imaging sensors. Proceedings of SPIE - The International Society for Optical Engineering Vol. 6232.
11. Gazit S, Szameit A, Eldar YC, Segev M (2009) Super-resolution and reconstruction of sparse sub-wavelength images. Optics Express 17:23920.
12. Brady DJ, Choi K, Marks DL, Horisaki R, Lim S (2009) Compressive holography. Optics Express 17:13040–13049.
13. Katz O, Bromberg Y, Silberberg Y (2009) Compressive ghost imaging. Appl. Phys. Lett. 95:131110.
14. Wu Y, Ye P, Mirza IO, Arce GR, Prather DW (2010) Experimental demonstration of an optical-sectioning compressive sensing microscope (CSM). Opt. Express 18:24565– 24578.
15. Candes E, Romberg J (2007) Sparsity and incoherence compressive sampling. Inverse problems 23:969–985.